Topological defects in open superconducting nanotubes after gradual and abrupt switching of the transport current and magnetic field

I. Bogush [1,2,3,*] and V. M. Fomin [1,3,4,†]

[1]*Institute for Integrative Nanosciences, Leibniz IFW Dresden, Helmholtzstraße 20, D-01069 Dresden, Germany*
[2]*Faculty of Physics, Lomonosov Moscow State University, 119899 Moscow, Russia*
[3]*Moldova State University, strada A. Mateevici 60, MD-2009 Chişinau, Republic of Moldova*
[4]*Institute of Engineering Physics for Biomedicine,*
National Research Nuclear University "MEPhI," Kashirskoe shosse 31, 115409 Moscow, Russia

We analyze dynamics of the order parameter in superconductor open nanotubes under a strong transport current in an external homogeneous magnetic field using the time-dependent Ginzburg-Landau equation. Near the critical transport current, the dissipation processes are driven by vortex and phase-slip dynamics. A transition between the vortex and phase-slip regimes is found to depend on the external magnetic field only weakly if the magnetic field and/or transport current are switched on gradually. In the case of an abrupt switch-on of the magnetic field or transport current, the system can be triggered to the stable phase-slip regime within a certain window of parameters. Finally, a hysteresis effect in the current-voltage characteristics is predicted in superconductor open nanotubes.

I. INTRODUCTION

Topological objects are indestructible by smooth transformations, and thus their stability is protected by topological considerations [1]. Topological defects in a superconductor, where the order parameter vanishes, may lead to the emergence of a finite resistance. The well-known topological defects are *vortices* in a bulk superconductor. The centerline of a vortex is called a vortex core, where the order parameter amplitude is zero and its phase is not defined. Encircling the vortex core along an arbitrary path gives a quantized phase change $2\pi n$ with an integer winding number $n \in \mathbb{Z}$.

The concept of the *phase slippage* was introduced for the resistive state of the narrow quasi-one-dimensional superconductor filaments in Ref. [2]. At the phase-slip event in a one-dimensional (1D) nanowire, the order parameter vanishes at some point, and the phase suffers a jump equal to 2π. There are various mechanisms of the phase-slip occurrence, e.g., the Langer-Ambegaokar-McCumber-Halperin (LAMCH) mechanism of thermal-dominated fluctuation-driven regime near the critical temperature [2,3], inhomogeneity-driven phase slip [4], and quantum phase slip [5].

Quantum phase slip in a two-dimensional (2D) superconductor has been recently found through magnetotransport measurements [6]. The 2D mechanism of phase-slip emergence related to unbinding of vortex-antivortex pairs below the Berezinski-Kosterlitz-Thouless (BKT) transition was developed in Refs. [7–9]. For nanowires of 100 nm, the LAMCH mechanism [2,10] was shown [11,12] to dominate over the

BKT transition at a relatively low current. In the interval of temperatures between the BKT critical temperature and the superconducting critical temperature, thermal fluctuations were sufficient to unbind vortex-antivortex pairs [13]. The BKT scenario was induced by a magnetic field in a 2D spin-dimer system with a multilayer magnet [14]. The BKT effect was revealed in a trapped quantum degenerate gas of rubidium atoms [15]. Another type of phase transition, a liquid-solid transition, was found experimentally in a 2D superconducting vortex system [16]. Bose-Einstein condensate in a three-dimensional (3D) optical lattice provided experimental evidence for the temperature-independent dissipation [17] as well as an ultracold quantum gas in 1D optical lattice did for the velocity-dependent dissipation [18]. The crossover between thermal and quantum phase slips controlled by velocity was detected in 1D superfluid tubes [19].

If the transport current is strong enough, the energy barrier for unbinding a vortex-antivortex pair can be overcome, and the thermally induced resistivity becomes dominant. In an external magnetic field, vortices move due to the Magnus force induced by transport current [20] and therefore contribute to resistivity. Even in a weak magnetic field, dissipation due to vortex movement dominates over the thermally activated phase-slip events in superconductor submicrometer wires [11].

Novel superconducting nanoarchitectures, e.g., open nanotubes [21–23] and nanocoils [24–26], provide new opportunities due to their complex geometry. If a nanotube is thin enough, only the component of the magnetic field normal to its surface plays a role in the order-parameter dynamics. This suggests making use of geometry to manipulate the effective magnetic field profile. As a result, the distribution of

---

*igbogush@gmail.com
†v.fomin@ifw-dresden.de

the order parameter is highly inhomogeneous, which opens the way to an interplay and transitions between vortex and phase-slip regimes. Fingerprints of the vortex and phase-slip patterns have been found in nanohelices with 100 nm diameter experimentally, supported by numerical simulations using the time-dependent Ginzburg-Landau (TDGL) equation [26]. In Ref. [27], a transition between different vortex and phase-slip patterns as a function of the transport current density and the external magnetic field has been revealed for niobium and tin open nanotubes with 400 nm radius. The complex profile of the magnetic field in open nanotubes introduces new features in the superconducting dynamics. For example, there exists the regime with two channels of the suppressed superconductivity along the nanotube with moving vortices, which cannot occur in a planar nanomembrane. Vortices in the half-cylinders move in opposite directions (while the vortex motion is unidirectional in an unfolded planar membrane) providing a qualitatively new feature. A planar nanostructure with a region of suppressed superconductivity contains one or a few chains of vortices moving in the same direction, while in a nanotube with phase slip, there are nucleating and annihilating vortex-antivortex pairs, which move towards each other [27]. The transition between Abrikosov-Josephson vortex and phase-slip regimes has been reported in a Josephson junction depending on the junction length and transport current [28]. However, the mechanism of the phase-slip occurrence is claimed to be attributed to the effective nonlocality in the order parameter dynamics, whilst the phase-slip in nanotubes emerges without nonlocality effects [27].

The hysteresis effects in superconductor magnetization occur due to surface currents, flux pinning, and the existence of different phases [29–31]. The hysteresis effects in current-voltage characteristics are found theoretically and experimentally in superconductor nanowires and microbridges [3,32–35]. The explanation of the hysteresis effect is attributed to the change of the effective temperature of quasiparticles due to the Joule heating [36–39] or the finite relaxation time of the order-parameter magnitude [32,40–45]. The hysteresis effect attributed to the phase-slip regime was described in a mesoscopic superconductor square with attached contacts [46] and NbN superconductor nanowires [47]. However, the hysteresis effect in these two systems appears due to the coupling of the order-parameter dynamics with the heat equation. When the system triggers the phase-slip regime, the normal current becomes larger, leading to a higher dissipation power and higher temperature of the sample. In its turn, a higher temperature of the sample favors the phase-slip regime, making the hysteresis effect appreciable. The hysteresis effect found in the present paper appears purely dynamically (due to the energy barrier between different superconducting regimes) at a constant temperature.

In the present paper, we push forward the studies of transitions between superconducting regimes in open nanotubes (Ref. [27]). While in Ref. [27], the superconductor nanotubes have been shown to demonstrate nontrivial behavior as a function of the external parameters (transport current density j_{tr} and magnetic field B), here we focus on the effect of the way of switch-on of those parameters. The dependency of the superconducting dynamics regime on the state preparation can be understood as a memory effect, which emphasizes the
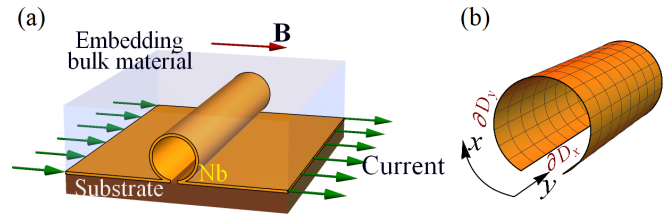

FIG. 1. (a) Scheme of the open nanotube embedded into a heat sink. (b) The coordinate system and boundaries of the open nanotube.

importance of the appropriate preparation both in experiment and in numerical simulations.

Section II represents the model based on the TDGL equations. In Sec. III, the induced voltage is shown to increase mainly monotonically with j_{tr} and B if they are switched on gradually. In Sec. IV, it is demonstrated that the abrupt transport current switch-on can cause a transition to the stable phase-slip regime, which is characterized by a higher induced voltage than the vortex regime. In Sec. V, a similar effect for the abrupt magnetic field switch-on is found. In Sec. VI, we investigate the hysteresis effect in current-voltage characteristics due to the stability of different dynamics regimes (particularly, phase-slip and vortex regimes). Sec.tion VII contains discussions of the obtained results and outlines their potential application.

II. MODEL

A physical model consists of a superconductor cylinder of a small thickness d with a small paraxial slit [Fig. 1(a)]. The cylinder is embedded in a heat sink, and the slit banks are connected to the contacts carrying a transport current. The cylinder is assumed to be thin enough in order to neglect the finite-thickness effects as discussed below. One of the prerequisites for applicability of the 2D approximation is that the induced magnetization has a negligible influence on the order parameter at other points across the wall (approximately, it can be expressed as $d < \lambda$, where λ is the penetration depth). Another applicability condition arises from the fact that the tangent magnetic field can lead to nucleation of vortices with cores across the cylinder wall. Thus, the cylinder should be thinner than the vortex diameter $\sim 4\xi$, where ξ is the coherence length. Also, we will neglect the impact of the induced magnetization of the cylinder. The condition of the applicability of this approximation is the Ginzburg-Landau (GL) parameter κ larger than some characteristic value as a function of d. Otherwise, the coupling between the electromagnetic field and the order parameter is strong, which modifies the order-parameter behavior both quantitatively and qualitatively [48,49]. The smallness of the effects of the induced magnetization and the tangent component of the magnetic field for Nb ($\kappa = 4.7$) C-shaped microdevice has been demonstrated in Ref. [50]. When all these conditions are met, the 3D equations of motion for the superconductor sample can be reduced to purely 2D ones.

Further in the present paper, we consider an infinitely thin superconductor cylinder D of radius R, length L with a slit of an arc length δ. The cylinder allows for a parametrization in two Cartesian coordinates: the arc length in the azimuthal

TABLE I. Materials and geometric parameters used for the simulations (see Ref. [27] for details; the dirty limit is used).

	Denotation	Value for Nb
Relative temperature	T/T_c	0.95/0.952/0.955
Penetration depth	$\lambda = \lambda_0\sqrt{\xi_0/[2.66(1 - T/T_c)]}$	273/278/287 nm
Coherence length	$\xi = 0.855\sqrt{\xi_0 l/(1 - T/T_c)}$	58/60/62 nm
GL parameter	$\kappa = \lambda/\xi$	4.7
Fermi velocity	$v_F = \sqrt{2E_F/m_e}$	6×10^{-5} m/s
Thickness of the film	d	50 nm
Mean free electron path	l	6.0 nm
Diffusion coefficient	$D = lv_F/3$	1.2×10^{-3} m^2/s
Normal conductivity of a thin membrane	$\sigma = l/[3.72 \times 10^{-16}\ \Omega\,\text{m}^2]$	16 $(\mu\Omega\,\text{m})^{-1}$
Cylinder radius	R	390 nm
Length	L	5 μm

direction $x \in [\delta/2, 2\pi R - \delta/2]$ and the coordinate along the axis $y \in [0, L]$ [Fig. 1(b)]. Such a cylinder can be bent from a flat membrane with a width $W = 2\pi R - \delta$. The cylinder is placed in a homogeneous magnetic field $\mathbf{B} = Be_z$. The magnetic field component tangent to the cylinder surface does not influence superconducting dynamics. Therefore, only the normal component $B_n = (\mathbf{B} \cdot \mathbf{n})$ (with a unit vector $\mathbf{n}$ normal to the cylinder surface) should be taken into consideration.

Following Ref. [27], we use a 2D TDGL dimensionless equation in the external magnetic field (see Tables I, II),

$$(\partial_t + i\kappa\varphi)\psi = \frac{1}{\kappa^2}(\nabla - i\kappa\mathbf{A})^2\psi + (1 - |\psi|^2)\psi, \quad (2.1)$$

where t is time, the vector potential $\mathbf{A}$ describes the magnetic field normal to the cylinder surface $B_n\mathbf{n} = [\nabla \times \mathbf{A}]$, the scalar potential φ describes the electric field $\mathbf{E} = -\nabla\varphi$, and the complex scalar field ψ is the order parameter. The continuity equation of the total current density (superconducting + normal) $\nabla \cdot (\mathbf{j}_{sc} + \mathbf{j}_n) = 0$ leads to the Poisson equation for the scalar potential φ:

$$\Delta\varphi = \frac{1}{\sigma}\nabla \cdot \mathbf{j}_{sc}, \quad \mathbf{j}_{sc} = \frac{1}{2i\kappa}[\psi^*(\nabla - i\kappa\mathbf{A})\psi - \text{c.c.}],$$
$$\mathbf{j}_n = \sigma\mathbf{E}, \quad (2.2)$$

where σ is the normal conductivity. Absence of the induced magnetization in our model allows us to exclude κ from the GL and Poisson equations (and the corresponding boundary conditions) through the following transformations: $x \to x/\kappa$, $\varphi \to \varphi/\kappa$, $B \to \kappa B$. We will keep κ in our equations for the sake of convenience. However, it is worth noticing that all results of the present paper are fair for other systems, which

can be obtained by the above transformations, if they meet the aforementioned conditions of the model applicability.

In the boundary conditions for the GL equation [20,51]

$$\mathbf{n} \cdot (\nabla - i\kappa\mathbf{A})\psi = -\frac{1}{b}\psi, \quad (2.3)$$

$b \to \infty$ corresponds to an insulator, a finite b applies for normal metals, and b approaches 0 for a magnetic material. For our purposes, we assume that $b \to \infty$ at free boundaries and $b = 0$ at the contacts:

$$(\partial_y - i\kappa A_y)\psi|_{\partial D_y} = 0, \quad \psi|_{\partial D_x} = 0, \quad (2.4)$$

where ∂D_x and ∂D_y are boundaries corresponding to the ends of the intervals for x and y, respectively [Fig. 1(b)]. The transport current density $\mathbf{j}_{tr}$ is introduced through the boundary conditions on the scalar potential

$$\partial_y\varphi|_{\partial D_y} = 0, \quad \partial_x\varphi|_{\partial D_x} = -j_{tr}/\sigma. \quad (2.5)$$

Integration schemes that are not gauge invariant may introduce large errors in numerical simulations. To avoid this issue, we use the link variables [52]

$$U_x^{ba} = \exp\left(-i\kappa \int_{x_a}^{x_b} A_x(x', y)dx'\right),$$
$$U_y^{ba} = \exp\left(-i\kappa \int_{y_a}^{y_b} A_y(x, y')dy'\right),$$
$$U_t^{ba} = \exp\left(i\kappa \int_{t_a}^{t_b} \varphi(t', x, y)dt'\right). \quad (2.6)$$

For the purposes of the numerical calculation, the integral for the link between two points of the spatial grid is approximated through a middle-point value of the integrand:

$$U_x^{ba} \approx \exp\left[-i\kappa A_x\left(\frac{x_a + x_b}{2}, y\right)\Delta x\right],$$
$$U_y^{ba} \approx \exp\left[-i\kappa A_y\left(x, \frac{y_a + y_b}{2}\right)\Delta y\right]. \quad (2.7)$$

When solving the Poisson equation, we take into account the fact that the speed of light is much higher than the speed of any other process involved in the order-parameter dynamics, such as the vortex velocity (light travels along the cylinder axis during $\sim$0.02 ps). This allows us to solve the elliptic equation with the Laplace operator instead of the hyperbolic

TABLE II. Units for the dimensionless quantities.

	Unit	Value for Nb at $T/T_c = 0.95$ [27]
Time	ξ^2/D	2.8 ps
Length	λ	273 nm
Magnetic field	$\Phi_0/2\pi\lambda\xi$	20.6 mT
Current density	$\hbar c^2/8\pi^2\lambda^2\xi e$	60 GA m^{-2}
Electric potential	$\sqrt{2}H_c\lambda^2/c\tau$	540 μV
Conductivity	$c^2/4\pi\kappa^2 D$	31 $(\mu\Omega\,\text{m})^{-1}$

one with the d'Alembert operator, which is advantageous for numerical calculation. The solution of the Poisson equation provides the value of the scalar potential φ exactly at the same instant, when we know the value of the order parameter ψ and the corresponding superconducting current density. So, we have to use this instantaneous value in the numerical link variable

$$U_t^{ab} = \exp\left[i\kappa\varphi(t,x,y)\Delta t\right] \quad (2.8)$$

instead of the middle-point value. Finally, to get the finite-difference scheme, the following rules

$$(\partial_x - i\kappa A_x)\psi \approx \frac{U_x^{ab}\psi_a - \psi_b}{\Delta x},$$

$$(\partial_x - i\kappa A_x)^2\psi \approx \frac{U_x^{ab}\psi_a - 2\psi_b + U_x^{cb}\psi_c}{(\Delta x)^2} \quad (2.9)$$

and similar rules for y and t are used. In order to construct an explicit numerical scheme, we use the approximations (2.9) and solve the TDGL equation (2.1) for the next time step

$$\psi(t+\Delta t) = \left(U_t^{t+\Delta t,t}\right)^{-1}\left\{\psi(t) + F\left[\psi, U_x^{ab}, U_y^{ab}\right]\Delta t\right\}, \quad (2.10)$$

where $F[\psi, U_x^{ab}, U_y^{ab}]$ is the right-hand side of Eq. (2.1) approximated through the link variables.

The voltage between the contacts is estimated as an averaged difference of the scalar potentials

$$U = \frac{1}{Lt_1}\int_{t_0}^{t_0+t_1}dt\int_0^L dy[\varphi(t,W,y) - \varphi(t,0,y)] \quad (2.11)$$

starting from some time t_0 during an interval t_1, which is much larger than any characteristic time of the dynamic processes in the system, such as the vortex nucleation period and its time of flight along the cylinder. The evolution is considered stationary and stable if the system demonstrates a quasiperiodic behavior (in terms of free energy, voltage as well as visual patterns of $|\psi|$, $\arg\psi$, and potential) for the time much longer than the aforementioned characteristic times. For numerical calculations, we exploit the finite-difference method with a grid containing 192 (along the x axis) $\times$ 384 (along the y axis) points and a time step $\Delta t = 0.03$ ps. A set of calculations performed with a finer grid and a shorter time step guarantees that the resulting evolution of the order parameter is stable.

We solve the Poisson equation using the iterative method after each step of the numerical solution for the order parameter. The stopping criterion for the iterative solver is the given smallness of the residual: $\max_{x,y}|\Delta\varphi - \frac{1}{\sigma}\nabla\cdot\mathbf{j}_{sc}| < \varepsilon$. The expression inside the modulus is a difference between the left-hand and right-hand sides of Eq. (2.2). The iterative method solves the Poisson equation until the absolute value of this difference is smaller than a chosen ε for all points of the grid. In addition, the solver performs at least ten iterations even if the stopping criterion has already been satisfied. In order to optimize the calculations, we choose $\varepsilon = 0.02$ since a further increase of the precision does not change the resulting evolution quantitatively. We use the previous solution for φ as a seed solution for the next time step to accelerate the calculations.

The iterative method for the Poisson equation works like that for the heat equation: the residual blurs out in the numerical solution with each iteration. As a result, if the boundary conditions are changed, one should perform as many iterations as needed to spread numerical corrections from one side of the grid to the opposite. In this case, the number of required iterations is of the order of the number of the grid points along the x axis ($\sim$200). Since this number is large, we make use of the standard methods of the partial differential equations to simplify the problem analytically (similarly to Ref. [53]). We represent the sought solution for the scalar potential as a sum $\varphi = \varphi_{dl} + \varphi_{\text{ind}}$ of two parts, φ_{dl} and φ_{ind}, satisfying the following equations:

$$\Delta\varphi_{dl} = 0, \quad \partial_y\varphi_{dl}|_{\partial D_y} = 0, \quad \partial_x\varphi_{dl}|_{\partial D_x} = -j_{tr}/\sigma, \quad (2.12)$$

$$\Delta\varphi_{\text{ind}} = \frac{1}{\sigma}\nabla\cdot\mathbf{j}_{sc}, \quad \mathbf{n}\cdot\nabla\varphi_{\text{ind}}|_{\partial D} = 0. \quad (2.13)$$

The first part, φ_{dl}, represents the nondivergent normal current density, and the second part, φ_{ind}, is the potential induced by the superconducting current density. The analytical expression for the first part is

$$\varphi_{dl} = -j_{tr}(x - \pi R)/\sigma, \quad (2.14)$$

and only the second part, φ_{ind}, remains to be calculated numerically.

The numerical algorithm is implemented in CUDA C $++$ [54] (with a wrapper written in Rust language [55]) in order to exploit the advantages of the high parallelism of graphical processing units.

III. GRADUAL CURRENT RAMPING

A naive expectation that the voltage between the contacts of the cylinder grows monotonically as a function of the magnetic field and transport current density turns out to be false. It has been shown [27] that a peak of the induced voltage $U(B, j_tr)$ emerges over a narrow interval of the external parameters due to the topological transitions between the vortex and phase-slip regimes. Those numerical experiments have been performed following these steps: prepare an initial random state of the order parameter, switch on the magnetic field, and after a relaxation (typically, $\sim$80 ps) switch on the transport current instantly. When the transport current is switched on, the vortex pattern, which has occurred in the external magnetic field, undergoes changes and adapts to the new conditions. If the transport current is switched on fast enough, the order parameter may suffer the impact of a high normal current density and come up with a metastable state containing a phase-slip line. It will be shown hereinafter, that the voltage peaks may occur due to the relaxation of the superconducting system to a metastable state in the regime of an abrupt switch-on of the transport current. An energy barrier between the phase-slip and vortex regimes can prevent the superconducting system from returning to the vortex regime. A similar effect can be achieved when the magnetic field is switched on abruptly after the transport current has been switched on.
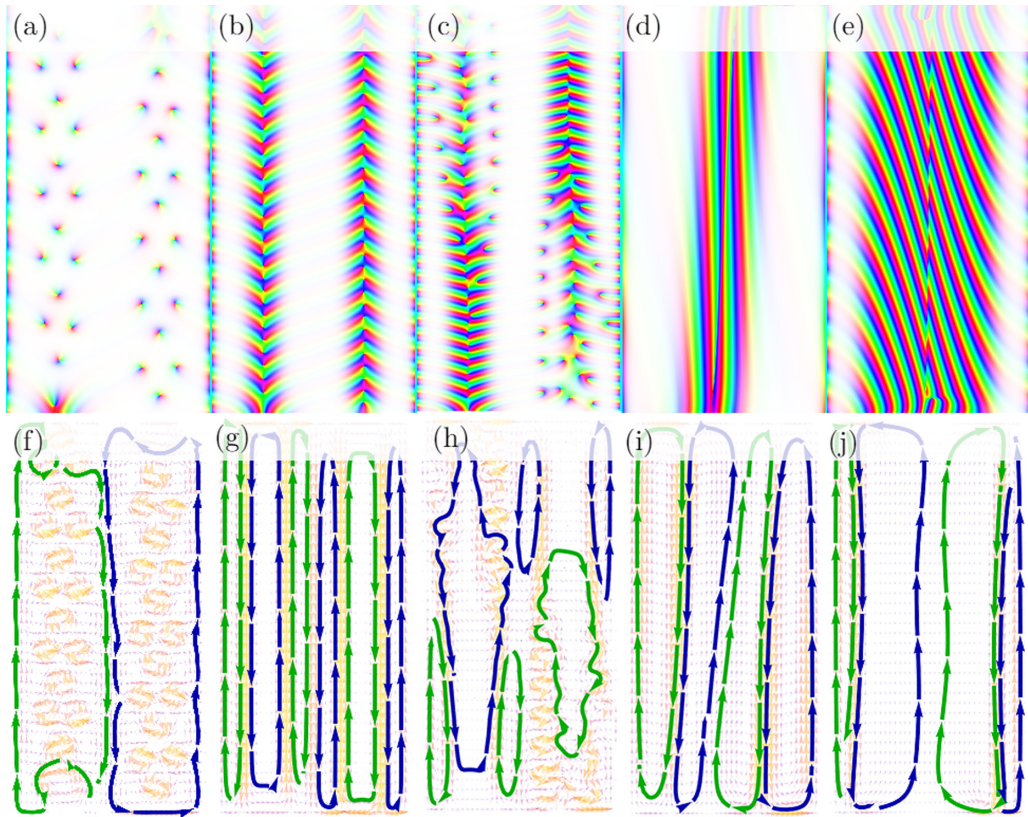
FIG. 2. Examples of the regimes depicted for the order parameter (upper panels) and total screening current density (lower panels) at $T/T_c = 0.952$. Each panel represents the unfolded open nanotube with height $L = 5 \, \mu$m and the membrane width $W = 2.39 \, \mu$m. From left to right: vortex lattice [(a), (f) $j_{tr} = 18$ GA/m^2, $B = 12.5$ mT], dense vortex chain [(b), (g) $j_{tr} = 20$ GA/m^2, $B = 20$ mT], dense vortex chain decaying into separate vortices [(c)(h) $j_{tr} = 18$ GA/m^2, $B = 35$ mT], a weak phase slip [(d),(i) $j_{tr} = 21$ GA/m^2, $B = 2.5$ mT], a strong phase slip [(e), (j) $j_{tr} = 22$ GA/m^2, $B = 10$ mT] . Current flows are obtained by numerical integration of the total screening current density. Green (blue) flows are clockwise (counterclockwise). Orange vectors stand for the vector field of the total screening current density. Color map of complex values is defined in Fig. 3.

The time of the linear switching on (ramping) of the transport current Δt_c or magnetic field Δt_f will be called the *ramp time* of the corresponding external parameter.

The numerical experiment with a gradual ramping of the current consists of the following steps.

(S1) Initialize the system with $\psi = 1 + 5 \times 10^{-3}(a + ib)$ and $\varphi = 0$, where a, b are random real numbers distributed normally as $\mathcal{N}(0, 1)$.

(S2) Switch on the magnetic field linearly from 0 to B during 10 ps.

(S3) Let the system relax during 100 ps.

(S4) Switch on the transport current density linearly from 0 to j_{tr} during $\Delta t_c = 500$ ps (in some calculations, we took even longer transport current ramp time Δt_c up to 10 ns in order to achieve a better convergence to the stationary state or to provide necessary gradualness of the ramping). Parameter values achieved at this step will be called "final."

(S5) Let the system come to the final (quasi-)stationary regime during 6–9 ns (for some calculations—up to 60 ns, if the state does not converge to a stationary one for a long time).

Under a low magnetic field and a weak transport current density, there are no vortices and phase slips in the open nanotube. However, the current injected from the contacts is normal, which generates the contact voltage (the contact resistance can be estimated from the results at $B = 0$ for a superconducting state without topological defects $U/j_{tr} \approx 11 \, \text{k}\Omega \, \text{m}^2$). When the transport current density approaches its critical value, and the magnetic field is high enough to lead to nucleation of vortices, dynamics of the topological defects become qualitatively richer. There are three main regimes in addition to their intermediate states. For weak current density and/or low magnetic fields, the first regime reveals a fragment of the *vortex lattice* with clearly manifested separate vortex cores in each half-cylinder [Figs. 2(a) and 2(f)]. The second regime occurs for stronger current density and higher magnetic fields. It is characterized by two channels of suppressed superconductivity in each half-cylinder with vortices, which travel in each channel and form *dense vortex chains* [Figs. 2(b) and 2(g)]. In order to distinguish two of these regimes, we introduce the definitions of *sparse* and *dense* vortex patterns. The vortex pattern is *sparse* if vortices are distinctly separated from each other and the amplitude $|\psi|$ forms a vortex core with the radius of the order of ξ. The vortex pattern is *dense* if vortices move inside the region of suppressed superconductivity. If the magnetic field is further increased, such channels with vortex chains can decay into separate vortices traveling in the half-cylinders [Figs. 2(c) and 2(h)]. The third regime is
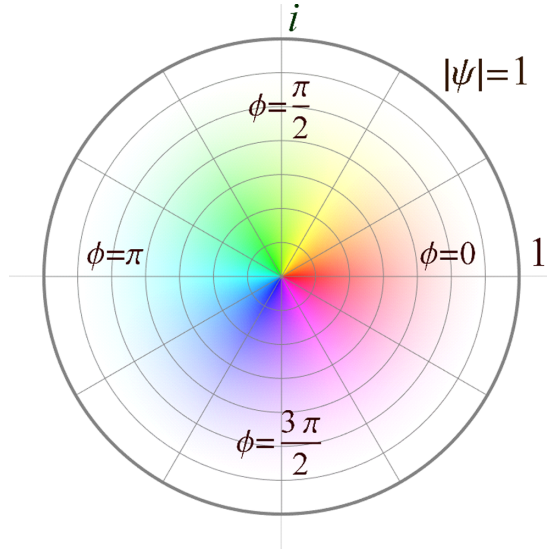
FIG. 3. Color map of the complex plane used for the presentation of the complex order parameter. The white color stands for a superconducting state $|\psi| \approx 1$ and more saturated colors stand for suppressed superconductivity. The color encodes the order-parameter phase.
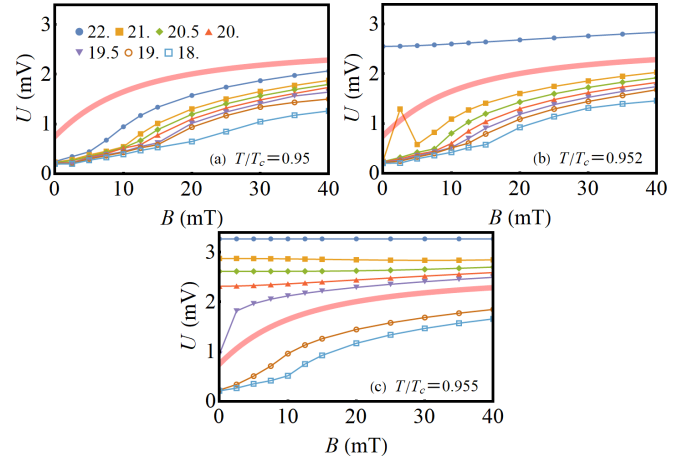

FIG. 4. Average voltage induced in Nb open nanotubes with $R = 390$ nm and slit $\delta = 60$ nm in the external magnetic field B at a gradually switched on transport current density j_{tr}. Different curves correspond to different values of j_{tr} (in GA/m^2). The transport current ramp time is $\Delta t_c = 500$ ps (and longer, for some points up to 10 ns). The pink bold line that separates vortex and phase-slip regimes is drawn manually.

distinguished by a *phase-slip* line in the region of the cylinder opposite to the slit, where vortex-antivortex pairs quickly nucleate, move, and annihilate/denucleate [Figs. 2(d) and 2(i); see [27] for details]. For the still higher values of the transport current density, the region of the suppressed superconductivity expands practically over the entire cylinder and contains a phase slip [Figs. 2(e) and 2(j)]. According to the results of the numerical calculations, a transition from the vortex to the phase-slip regime is accompanied by a voltage jump, since the latter regime is characterized by a higher voltage than the former one.

The results for different relative temperatures T/T_c are depicted in Fig. 4. The transition between the vortex regime with a lower voltage and a phase-slip regime with a higher voltage occurs at some value of j_{tr}, which decreases with rising temperature. The approximate boundary between the vortex and phase-slip regimes is at around 2 mV, except for the case of low magnetic fields, when the phase-slip regime is characterized by a lower voltage (e.g., 1 mV for $T/T_c = 0.955$, $j_{tr} = 19.5$ GA/m^2, $B = 0$). The transition to the phase-slip regime does not depend on the magnetic field B, except one peak at $T/T_c = 0.952$, $j_{tr} = 21$ GA/m^2, $B = 2.5$ mT, which will be discussed at the end of the present section.

When the system implements the regime with vortex chains inside a band of suppressed superconductivity, this band appears in a region with a maximal normal magnetic field. We suggest a simple model by considering that a point of the cylinder is in a perfect superconducting state if the normal magnetic field is lower than some conventional characteristic value B_1. Otherwise, it conducts normal current and possesses normal conductivity σ. In this case, the fraction of the cylindrical surface, where the normal magnetic field is smaller than B_1, is arccos(B_1/B). Consequently, the induced voltage can be

estimated as

$$U_{\text{est}} = \frac{4jR}{\sigma}\arccos\frac{B_1}{B}, \tag{3.15}$$

and the function

$$b_U = \left(\cos\frac{\sigma U}{4jR}\right)^{-1} \tag{3.16}$$

applied to the numerical results should behave linearly as a function of B in this regime. Generally, the plots for $T/T_c = 0.95$, 0.952 are indeed piecewise linear (Fig. 5). Besides that, the plots contain kinks, indicating changes of the regime. For example, in the plot for $j_{tr} = 19$ GA/m^2, $T/T_c = 0.95$, there are two kinks, at $B = 15$ and 30 mT. The superconducting state contains fragments of a vortex lattice—below 15 mT, two narrow dense vortex chains in bands with suppressed superconductivity—from 15 to 30 mT, and dense vortex chains, decaying into separate vortices—above 30 mT.

A transition between the vortex and phase-slip regimes does not occur when raising the magnetic field (at a constant transport current density), except for the voltage peak at $T/T_c = 0.952$, $j_{tr} = 21$ GA/m^2, and $B = 2.5$ mT. This peak survives even if the transport current is switched on with the ramp time $\Delta t_c = 100$ ns. It disappears at a slightly weaker transport current density $j_{tr} = 20.95$ GA/m^2, and the phase slip is manifested over the whole analyzed range of the magnetic fields at $j_{tr} = 21.5$ GA/m^2. Therefore, the transition to the phase-slip regime under a gradually switched on transport current occurs only in a narrow window of parameters around the above-mentioned values. In order to describe the mechanism leading to this peak, notice that the 2.5 mT magnetic field is strong enough for nucleation of vortices (which have different vorticity in two half-cylinders). On one hand, the magnetic field makes the state with vortices arranged in the regions with a maximal magnitude of the magnetic field more preferable. On the other hand, the interaction between vortices
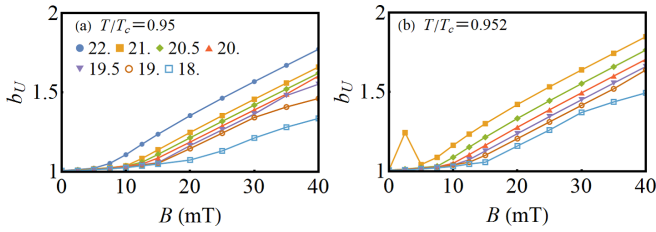
FIG. 5. Function b_U of Eq. (3.16) constructed for plots in Fig. 4.

with different vorticity forces them to attract each other. If the latter attraction is energetically dominant over the above-described arrangement, then vortices are pushed toward the line opposite to the slit and form a phase slip, which results in a voltage peak.

In the vortex regime, the nucleation and denucleation of moving vortices give rise to voltage oscillations (typically ranging from 10 to 30 GHz). In low magnetic fields (~ 2 mT), only several vortices are present at every instant. This results in a lower frequency and higher amplitude of the voltage oscillations with respect to the average voltage (a larger modulation depth). For example, the system at $T/T_c = 0.952$, $j_{tr} = 20$ GA/m^2, $B = 2$ mT generates a nonharmonic periodic 8.7 GHz signal oscillating with $\sim 10\%$ modulation depth.

IV. METASTABLE STATES INDUCED BY AN ABRUPT TRANSPORT CURRENT RAMPING

Depending on the transport current ramping, the superconducting nanotube can arrive at either phase-slip or vortex regime, demonstrating a stable and (quasi-)periodic stationary evolution. In the present section, we analyze the abrupt transport current ramping.

Reduction of the transport current ramp time to $\Delta t_c = 10$ ps leads to the occurrence of new peaks in the magnetic field–voltage diagrams (Fig. 6). The narrowness of the ramping, which is needed to get a phase-slip regime, decreases if one approaches the critical current density (see, e.g., $T/T_c = 0.95$, $B = 10$ mT in Fig. 7). These peaks correspond to the phase-slip regime induced by an abrupt transport current ramping, while in the case of a gradual current switch-on, there are two vortex chains. Temporal stability of the phase-slip regime triggered by the abrupt transport current ramping is confirmed by obtaining it for the $T/T_c = 0.952$, $B = 10$ mT, $j_{tr} = 20$ GA/m^2, $\Delta t_c = 20$ ps during 60 ns.

The difference between the order-parameter evolution types at gradual and abrupt transport current ramping is represented in Fig. 8. For the gradual current ramping, the superconducting system has enough time to adapt to a higher transport current density, so that new vortices nucleate in both half-cylinders [Figs. 8(a)–8(e)]. This ends up with two dense vortex patterns [Fig. 8(e)]. For the abrupt current ramping [Figs. 8(f)–8(j)], the system does not manage to nucleate new vortices fast enough in response to the transport current growth. This promotes suppression of superconductivity in the region opposite to the cylinder slit [Fig. 8(h)]. The region with suppressed superconductivity grows and captures the vortices
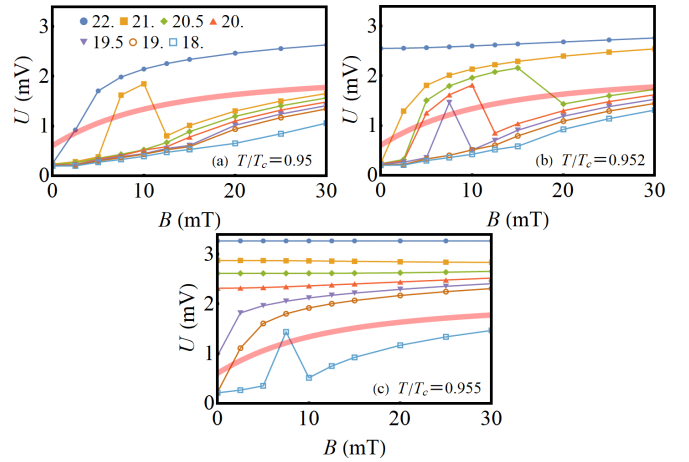

FIG. 6. Average voltage induced in Nb open nanotubes with $R = 390$ nm and slit $\delta = 60$ nm in the external magnetic field B and at a transport current density j_{tr}, which is switched on abruptly during $\Delta t_c = 10$ ps. Different curves correspond to different values of j_{tr} (given in GA/m^2 next to the corresponding symbols). The pink bold line is drawn manually and separates vortex and phase-slip regimes schematically.

from the half-cylinders [Fig. 8(i)]. Vortex chains from both half-cylinders begin moving toward the line opposite to the cylinder slit, and finally, they come up with a vortex-antivortex chain constituting the phase-slip line [Fig. 8(j)]. For the intermediate ramping, if the narrowness of the ramping is not enough to promote formation of a phase slip, the region of suppressed superconductivity does not grow, but rather decays into several vortex-antivortex pairs, which join the vortex chains in both half-cylinders.

V. METASTABLE STATES INDUCED BY ABRUPT MAGNETIC FIELD RAMPING

A similar effect can be achieved if first the transport current and then the magnetic field are switched on. Our calculations with a gradual ramping of both the magnetic field and transport current exhibit the superconducting behavior similar to that discussed in Sec. III. An abrupt magnetic field ramping with the magnetic field–ramp time $\Delta t_f = 10$ ps gives rise to a
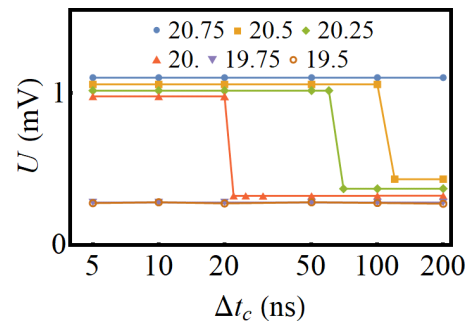

FIG. 7. Average voltage induced in Nb open nanotubes with $R = 390$ nm, $\delta = 60$ nm, $T/T_c = 0.95$, $B = 10$ mT as a function of the transport current ramp time Δt_c at different values of j_{tr} (given in GA/m^2 next to the corresponding symbols).
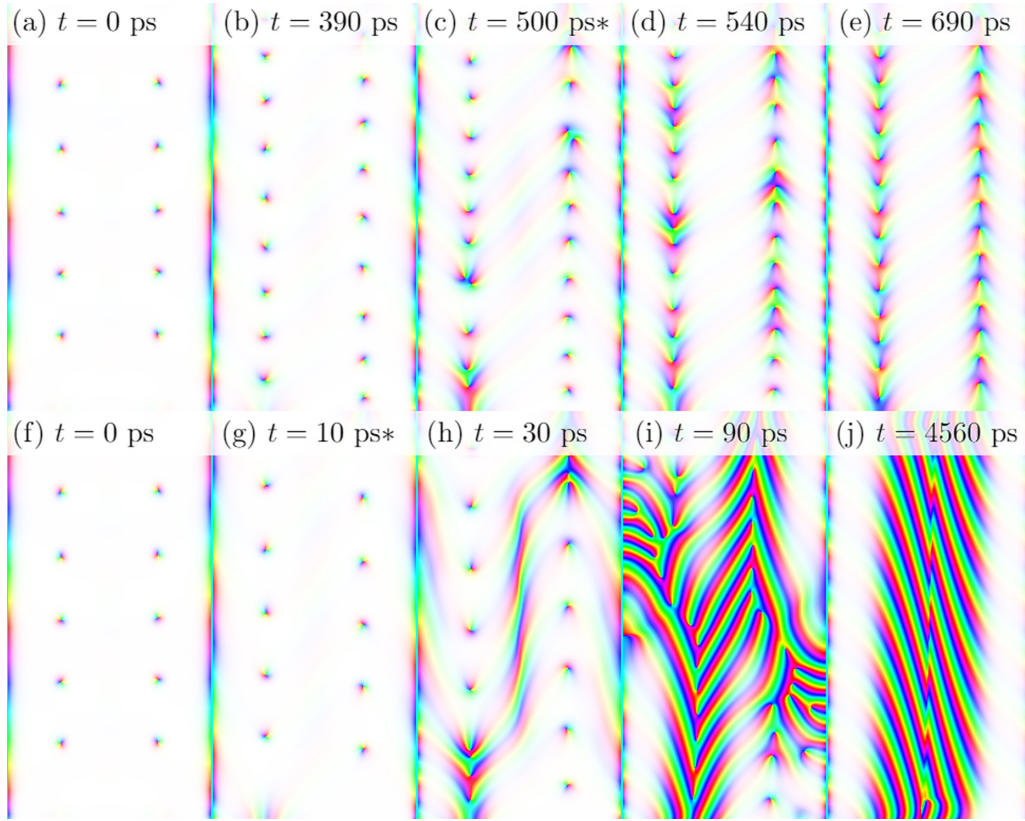
FIG. 8. Order-parameter snapshots for $R = 390$ nm, $T/T_c = 0.952$, $B = 10$ mT, $j_{tr} = 20.5$ GA/m^2 for two transport current ramp times Δt_c: gradual ramping $\Delta t_c = 500$ ps (upper) and abrupt ramping $\Delta t_c = 10$ ps (lower). Each panel represents the unfolded open nanotube with height $L = 5$ μm and the membrane width $W = 2.39$ μm. Time t is counted from the moment when the transport current begins to switch on and indicated in the frames. The asterisk denotes the frames (c) and (g), when the transport current density achieves its final values.

transition from the vortex to the phase-slip regime as reflected in the magnetic field–voltage characteristics (Fig. 9).
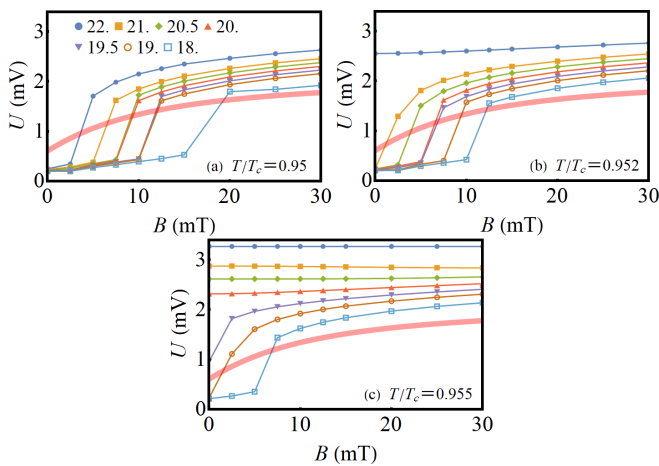

FIG. 9. Average voltage induced in Nb open nanotubes with $R = 390$ nm and slit $\delta = 60$ nm, when first the transport current is switched on, and then the magnetic field is switched on abruptly. The magnetic field ramp time is $\Delta t_f = 10$ ps. Different curves correspond to different values of the transport current density j_{tr} (given in GA/m^2 near the corresponding symbols). The pink bold line is drawn manually and separates vortex and phase-slip regimes schematically.

If the transport current is switched on first, a gradual magnetic field ramping leads to the vortex regime [Figs. 10(a)–10(e)], and an abrupt magnetic field ramping leads to the phase-slip regime [Figs. 10(f)–10(j)] in the order-parameter evolution as depicted in Fig. 10. As the current density is subcritical, the state before the magnetic field is switched on does not contain any topological defects. For a gradual magnetic field ramping, a vortex chain nucleates in response to the magnetic field change [Figs. 10(a)–10(e)]. For an abrupt magnetic field ramping, the superconducting system does not manage to nucleate vortices as quickly as required by the rising magnetic flux, and the superconductivity is suppressed in the region opposite to the slit [in the middle of the panel, Fig. 10(h)]. In the region of suppressed superconductivity, vortices and antivortices nucleate, move, and annihilate/denucleate—a behavior typical of the phase-slip regime [Fig. 10(j)].

VI. HYSTERESIS IN THE CURRENT-VOLTAGE CHARACTERISTIC CONTROLLED BY THE MAGNETIC FIELD

As demonstrated in the previous sections, depending on the way in which the current or magnetic field is switched on, the system can arrive at different regimes for the same set of final parameters. This means that there is an appreciable energy barrier between those regimes of superconducting dynamics.
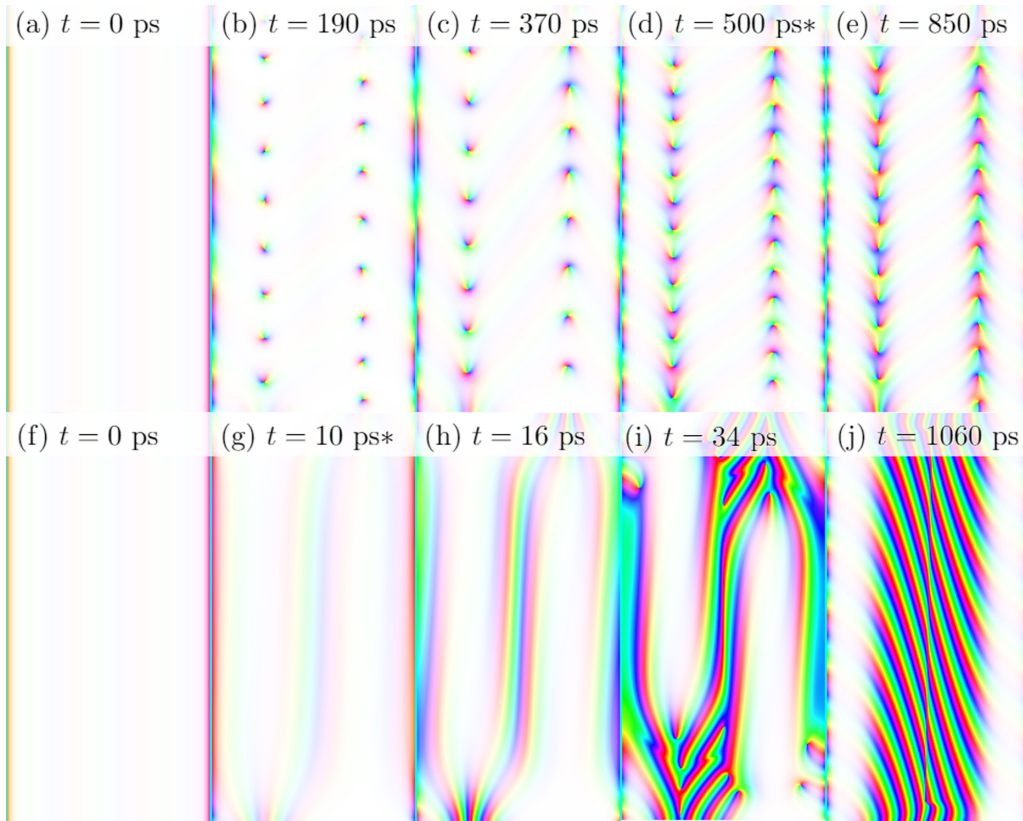
FIG. 10. Order-parameter snapshots for $R = 390$ nm, $T/T_c = 0.952$, $B = 10$ mT, $j_{tr} = 20.5$ GA/m^2 for different magnetic field ramp times Δt_f: gradual $\Delta t_f = 500$ ps (upper) and abrupt $\Delta t_f = 10$ ps (lower). Each panel represents the unfolded open nanotube with height $L = 5$ μm and the membrane width $W = 2.39$ μm. Time t is counted from the moment when the magnetic field begins to switch on. The asterisk denotes the frame, when the magnetic field achieves its final value [at Figs. 10(d) and 10(g)].

As a result, a hysteresis can occur. To analyze this effect, the following steps are performed:

(H1) Prepare an initial random state [in the same way as in (S1)].

(H2) Switch on the magnetic field linearly from 0 to its final value B during 10 ps and let the system relax during 100 ps.

(H3) Switch on the transport current density linearly from 0 to 14 GA/m^2 during 100 ps and let the system relax during 400 ps.

(H4) Increase j_{tr} by 0.129 GA/m^2 during 100 ps and let the system relax during 400 ps. Repeat this stage until j_{tr} reaches the value of 23 GA/m^2.

(H5) Repeat (H4) in the opposite direction, namely, decrease the transport current density from 23 to 14 GA/m^2.

The results of calculations conducted for $T/T_c = 0.952$ at different values of B are represented in Fig. 11. The hysteresis is practically negligible at $B = 0, 2.5$ mT. Actually, the apparent hysteresis for these values appears due to the short relaxation time (which is a computational restriction). Hence, there is no energy barrier between the phase-slip and the vortex regimes for the weak magnetic field. Starting from ∼5 mT, the hysteresis is distinctly manifested. The hysteresis loop is wider along j_{tr} and narrower along U for higher magnetic fields. As a result, the hysteresis loop area has a maximum at some value of the magnetic field B between 10 and 20 mT.

The hysteresis loop area can be interpreted as a power of excessive dissipation attributed to the existence of the higher branch of the loop in comparison with the process if only the lower branch would exist. In addition to the hysteresis, which is the result of transitions between the vortex and the phase-slip regimes, we have found a smaller hysteresis loop (see the burgundy frame in Fig. 11) for the transition between a sparse vortex lattice [Fig. 4(a)] and a dense vortex chain [Fig. 4(b)].
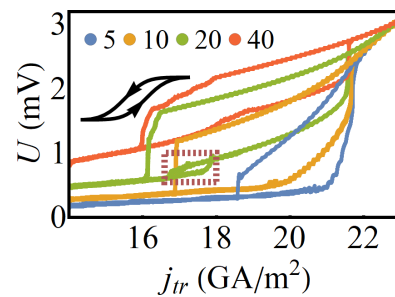

FIG. 11. Hysteresis in the current-voltage characteristic of Nb open nanotubes with $R = 390$ nm, $\delta = 60$ nm, $T/T_c = 0.952$ for different values of the magnetic field (indicated in mT near the corresponding symbols). The scheme in the inset shows the sequence of the voltage changes during steps (H4) and (H5) described in the text.

VII. DISCUSSIONS

We have shown that for the gradual switch-on of the magnetic field and/or transport current in the superconductor open nanotubes, the transition between the vortex and the phase-slip regimes depends on the magnetic field only weakly. Depending on the way of ramping, the superconducting nanotube can arrive at different regimes for the same final external parameters: the transport current density and magnetic field. Abrupt magnetic field or transport-current ramping can lead to the transition to the phase-slip regime. Therefore, the ramp time of the external stimuli can be used to control the vortex/phase-slip transition in the superconducting nanotubes. Consequently, we emphasize the importance of taking into account the realistic ramping of the external stimuli (e.g., transport current and external magnetic field) in numerical calculations.

The energy barrier between phase-slip and vortex regimes becomes bigger in higher magnetic fields. This barrier leads to the occurrence of appreciable hysteresis in the current-voltage characteristics controlled by the magnetic field. The superconducting state near the critical transport current density depends on the way by which the final external parameters are achieved, constituting a *memory effect*. Within our analysis, dependency of the superconducting regime on the ramping and the hysteresis appear dynamically, due to the energy barrier between different superconducting regimes, with no contribution of the heat-related effects.

The numerical simulation of superconducting dynamics demonstrates the voltage peak even for the gradual ramping in a narrow window of parameters near $T/T_c = 0.952$, $B = 2.5$ mT, $j_{tr} = 21$ GA/m^2. We conjecture that it appears when the magnetic field is strong enough to begin nucleating vortices, but the current-induced attraction between vortices in two half-cylinders is still energetically more preferable than the arrangement of vortices in the regions with a maximal magnitude of the magnetic field. Moreover, in the range of parameters where there are only a few vortices, 8.7 GHz alternating voltage is generated with a relatively large modulation depth ∼10%.

The presented results shed light on the interplay between different regimes of the superconducting dynamics in open nanotubes with clear perspectives for application in various fields of nanotechnology. An understanding of the transition between the vortex and phase-slip regimes helps manufacture nanosensors of the magnetic field as well as quantum-interference-based filters and switchers. The existence of the metastable states is promising to boost the progress in fluxon-based devices for quantum computing and to improve the performance of the nanostructured bolometers and terahertz detectors.

[1] H. Eschrig, *Topology and Geometry for Physics* (Springer, Berlin-Heidelberg, 2011).

[2] J. S. Langer and V. Ambegaokar, Phys. Rev. **164**, 498 (1967).

[3] R. Tidecks, *Current-Induced Nonequilibrium Phenomena in Quasi-One Dimensional Superconductors* (Springer, Berlin-Heidelberg, 1990).

[4] J. Skocpol, M. R. Beasley, and M. Tinkham, J. Low Temp. Phys. **16**, 145 (1974).

[5] N. Giordano, Phys. Rev. Lett. **61**, 2137 (1988).

[6] Y. Saito, T. Nojima, and Y. Iwasa, Nat. Commun. **9**, 778 (2018).

[7] V. S. Berezinskii, Zh. Exp. Teor. Fiz. **59**, 907 (1970) [Sov. Phys. JETP **32**, 493 (1971)].

[8] V. S. Berezinskii, Zh. Exp. Teor. Fiz. **61**, 1144 (1971) [Sov. Phys. JETP **34**, 610 (1972)].

[9] J. M. Kosterlitz and D. J. Thouless, J. Phys. C: Solid State Phys. **6**, 1181 (1973).

[10] D. E. McCumber and B. I. Halperin, Phys. Rev. B **1**, 1054 (1970).

[11] M. Bell, N. Kaurova, and A. Divochiy, IEEE Trans. Appl. Supercond. **17**, 267 (2007).

[12] M. Bell, A. Sergeev, V. Mitin, J. Bird, A. Verevkin, and G. Gol'tsman, Phys. Rev. B **76**, 094521 (2007).

[13] B. I. Halperin and D. R. Nelson, J. Low Temp. Phys. **36**, 599 (1979).

[14] U. Tutsch *et al.*, Nat. Commun. **5**, 5169, (2014).

[15] Z. Hadzibabic, P. Krüger, M. Cheneau, B. Battelier, and J. Dalibard, Nature (London) **441**, 1118 (2006).

[16] B. Chen, W. P. Halperin, P. Guptasarma, D. G. Hinks, V. F. Mitrović, A. P. Reyes, and P. L. Kuhns, Nat. Phys. **3**, 239 (2007).

[17] D. McKay, M. White, M. Pasienski, and B. DeMarco, Nature (London) **453**, 76 (2008).

[18] L. Tanzi, S. S. Abbate, F. Cataldini, L. Gori, E. Lucioni, M. Inguscio, G. Modugno, and C. D'Errico, Sci. Rep. **6**, 25965 (2016).

[19] S. S. Abbate, L. Gori, M. Inguscio, G. Modugno, and C. D'Errico, Eur. Phys. J.: Spec. Top. **226**, 2815 (2017).

[20] M. Thinkham, *Introduction to Superconductivity* (McGraw-Hill, New York, 1996).

[21] V. M. Fomin, R. O. Rezaev, and O. G. Schmidt, Nano Lett. **12**, 1282 (2012).

[22] R. O. Rezaev, E. A. Posenitskiy, E. I. Smirnova, E. A. Levchenko, O. G. Schmidt, and V. M. Fomin, Phys. Stat. Sol. Rapid Research Letters **13**, 1800251 (2019).

[23] M. I. Tsindlekht, V. M. Genkin, I. Felner, F. Zeides, N. Katz, S. Gazi, S. Chromik, and O. V. Dobrovolskiy, arXiv:2106.11694.

[24] V. M. Fomin, R. O. Rezaev, E. A. Levchenko, D. Grimm, and O. G. Schmidt, J. Phys.: Condens. Matter **29**, 395301 (2017).

[25] S. Lösch, A. Alfonsov, O. V. Dobrovolskiy, R. Keil, V. Engemaier, S. Baunack, G. Li, O. G. Schmidt, and D. Bürger, ACS Nano **13**, 2948 (2019).

[26] R. Córdoba, D. Mailly, R. O. Rezaev, and E. I. Smirnova, Nano Lett. **19**, 8597 (2019).

[27] R. O. Rezaev, E. I. Smirnova, O. G. Schmidt, and V. M. Fomin, Commun. Phys. **3**, 144 (2020).

[28] A. Sheikhzada and A. Gurevich, Phys. Rev. B **95**, 214507 (2017).

[29] D. G. Schweitzer, M. Garber, and B. Bertman, Phys. Rev. **159**, 296 (1967).

[30] D. G. Schweitzer and M. Garber, Phys. Rev. **160**, 348 (1967).

[31] D. G. Schweitzer, Phys. Rev. **173**, 461 (1968).

[32] S. Michotte, S. Matefi-Tempfli, L. Piraux, D. Y. Vodolazov, and F. M. Peeters, Phys. Rev. B **69**, 094512 (2004).

[33] D. Yu. Vodolazov and F. M. Peeters, Phys. Rev. B **84**, 094511 (2011).

[34] E. Segev, O. Suchoi, O. Shtempluck, F. Xue, and E. Buks, Appl. Phys. Lett. **98**, 052504 (2011).

[35] K. K. Likharev, Rev. Mod. Phys. **51**, 101 (1979).

[36] V. N. Gubankov, K. K. Likharev, and N. M. Margolin, Fiz. Tverd. Tela **14**, 953 (1972) [Sov. Phys. Solid State **14**, 819 (1972)].

[37] W. J. Skocpol, M. R. Beasley, and M. Tinkham, J. Appl. Phys. **45**, 4054 (1974).

[38] M. Tinkham, J. U. Free, C. N. Lau, and N. Markovic, Phys. Rev. B **68**, 134515 (2003).

[39] D. Hazra, L. M. A. Pascal, H. Courtois, and A. K. Gupta, Phys. Rev. B **82**, 184530 (2010).

[40] K. K. Likharev and L. A. Yakobson, Zh. Eksp. Teor. Fiz. **68**, 1150 (1975) [Sov. Phys. JETP **41**, 570 (1975)].

[41] Y. Song, J. Appl. Phys. **47**, 2651 (1976).

[42] H. Hojgaard-Jensen and P. E. Lindelof, J. Low Temp. Phys. **23**, 469 (1976).

[43] R. B. Van Dover, A. De Lozanne, and M. R. Beasley, J. Appl. Phys. **52**, 7327 (1981).

[44] A. Baratoff and L. Kramer, in *Proceedings of the International Conference on Superconducting Quantum Interference Devices and Their Applications* (Walter de Gruyter, Berlin, 1977), pp. 51–62.

[45] A. L. De Lozanne and M. R. Beasley, in *Nonequilibrium Superconductivity*, edited by D. N. Langenberg and A. I. Larkin (Elsevier, Amsterdam, 1986), Chap. 3.

[46] D. Y. Vodolazov, F. M. Peeters, M. Morelle, and V. V. Moshchalkov, Phys. Rev. B **71**, 184502 (2005).

[47] A. K. Elmurodov, F. M. Peeters, D. Y. Vodolazov, S. Michotte, S. Adam, F. de Menten de Horne, L. Piraux, D. Lucot, and D. Mailly, Phys. Rev. B **78**, 214519 (2008).

[48] E. H. Brandt, Phys. Rev. B **71**, 014521 (2005).

[49] E. H. Brandt, Phys. Rev. B **79**, 134526 (2009).

[50] E. I. Smirnova, R. O. Rezaev, and V. M. Fomin, Low Temp. Phys. **46**, 325 (2020).

[51] P. G. De Gennes, Superconductivity Of Metals And Alloys (Westview Press, Colorado, 1999).

[52] R. Kato, Y. Enomoto, and S. Maekawa, Phys. Rev. B **47**, 8016 (1993).

[53] I. A. Sadovskyy, A. E. Koshelev, C. L. Phillips, D. A. Karpeyev, and A. Glatz, J. Comput. Phys. **294**, 639 (2015).

[54] CUDA Toolkit Documentation v11.5.0, https://docs.nvidia.com/cuda/ (accessed November 10, 2021).

[55] The Rust Reference, https://doc.rust-lang.org/1.54.0/reference/ (accessed November 10, 2021).